BRAIN
A JOURNAL OF NEUROLOGY

Expression of *mitofusin 2*^{R94Q} in a transgenic mouse leads to Charcot–Marie–Tooth neuropathy type 2A

Romain Cartoni,[1] Estelle Arnaud,[2] Jean-Jacques Médard,[2] Olivier Poirot,[2] Delphine S. Courvoisier,[3] Roman Chrast[2,*] and Jean-Claude Martinou[1,*]

1 Department of Cell Biology, University of Geneva, 30 quai Ernest-Ansermet, 1211 Genève 4, Switzerland
2 Department of Medical Genetics, University of Lausanne, 27 Rue du Bugnon, 1005 Lausanne, Switzerland
3 Division of Clinical Epidemiology, Geneva University Hospitals, University of Geneva, rue Gabrielle Perret-Gentil 4, 1211 Genève 14, Switzerland

*These authors contributed equally to this work.

Correspondence to: Prof. Jean-Claude Martinou,
Department of Cell Biology,
University of Geneva,
30 quai Ernest-Ansermet,
1211 Genève 4, Switzerland
E-mail: jean-claude.martinou@unige.ch

Correspondence may also be addressed to: Asst. Prof. Roman Chrast,
Department of Medical Genetics,
University of Lausanne,
27 Rue du Bugnon,
1005 Lausanne, Switzerland
E-mail: roman.chrast@unil.ch

Charcot–Marie–Tooth disease type 2A is an autosomal dominant axonal form of peripheral neuropathy caused by mutations in the *mitofusin 2* gene. *Mitofusin 2* encodes a mitochondrial outer membrane protein that participates in mitochondrial fusion in mammalian cells. How mutations in this protein lead to Charcot–Marie–Tooth disease type 2A pathophysiology remains unclear. We have generated a transgenic mouse expressing either a mutated (R94Q) or wild-type form of human *mitofusin 2* in neurons to evaluate whether the R94Q mutation was sufficient for inducing a Charcot–Marie–Tooth disease type 2A phenotype. Only mice expressing *mitofusin 2*^{R94Q} developed locomotor impairments and gait defects thus mimicking the Charcot–Marie–Tooth disease type 2A neuropathy. In these animals, the number of mitochondria per axon was significantly increased in the distal part of the sciatic nerve axons with a diameter smaller than $3.5\,\mu m$. Importantly, the analysis of R94Q transgenic animals also revealed an age-related shift in the size of myelinated axons leading to an over-representation of axons smaller than $3.5\,\mu m$. Together these data suggest a link between an increased number of mitochondria in axons and a shift in axonal size distribution in *mitofusin 2*^{R94Q} transgenic animals that may contribute to their neurological phenotype.

Introduction

With an estimated prevalence of 1 in 2500 individuals, Charcot–Marie–Tooth (CMT) neuropathies (also called hereditary motor and sensory neuropathies) are among the most common inherited neurological disorders (Skre, 1974). CMT disease type 2A (CMT2A) is the axonal form of CMT disease, with clinical symptoms including progressive distal limb muscle weakness and atrophy, distal sensory loss and mobility impairment, which often lead to wheelchair dependency. A degeneration of the long peripheral axons appears to be the major event leading to the disorder especially in early onset symptomatic patients. In contrast, late onset symptomatic patients have been shown to present no detectable signs of axonal degeneration (Schröder, 2001; Chung *et al.*, 2006). Recently, a major advance in the comprehension of the disease has been reached when several studies identified mutations in the *mitofusin 2 gene (MFN2)* as responsible for CMT2A (Zuchner *et al.*, 2004; Kijima *et al.*, 2005; Chung *et al.*, 2006; Verhoeven *et al.*, 2006). MFN2 is a highly conserved large GTPase protein anchored in the outer mitochondrial membrane. Together with mitofusin 1 (MFN1), MFN2 plays a role in the fusion of the outer mitochondrial membrane in mammalian cells (for review, see Chan, 2006) through the formation of homo and/or hetero complexes (Detmer and Chan, 2007*a*). MFN1 and 2 are essential proteins since their inactivation in mice leads to mid-gestation lethality at E12.5 and E11.5, respectively (Chen *et al.*, 2003). Moreover, conditional deletion of only *Mfn2* is sufficient to cause degeneration of Purkinje cells in the cerebellum (Chen *et al.*, 2007). The cause for the degeneration of these cells is not yet clearly established. So far only a few studies have addressed the role of MFN2 mutations as the cause of CMT2A neuropathy. Motoneuron specific overexpression of the MFN2[T105M] mutated form leads to a severe and general axonal loss of motoneurons exclusively in young homozygote transgenic animals (Detmer *et al.*, 2008). However, unlike in patients where mitochondria tend to accumulate in axons (Verhoeven *et al.*, 2006; Vallat *et al.*, 2008; Funalot *et al.*, 2009) the mitochondria aggregate around the nucleus and are absent from axons of motoneurons in T105M transgenic mice. Similar data were obtained when MFN2 proteins with mutations found in CMT2A disease were overexpressed in cultured rat neurons from dorsal root ganglion (Baloh *et al.*, 2007). While potentially interesting, the relevance of MFN2-induced perinuclear mitochondrial aggregation for the pathophysiology of CMT2A disease is difficult to interpret since this phenomenon has been observed when the level of MFN2 overexpression was high (Eura *et al.*, 2003; Detmer and Chan, 2007*b*).

To investigate the role of *MFN2* mutations in the physiopathology of CMT2A further, we generated two lines of transgenic mice expressing the mutated form of human MFN2[R94Q] specifically in neurons under the control of a neuron specific enolase promoter. This mutation was selected since the arginine at position 94 has been reported to be the most commonly mutated residue in CMT2A patients (Cartoni and Martinou, 2009). As a control, we generated a transgenic mouse expressing wild-type MFN2 also under the control of the neuron specific enolase promoter. Here,

we describe the phenotype of these mice and report that *MFN2*[R94Q] transgenic mice display clinical and pathophysiological symptoms that closely mimic those seen in patients suffering from CMT2A.

Materials and methods

Generation of transgenic MitoCharc mice

This work was approved by the Health Department of the State of Geneva. All experiments were carried out accordingly to good practice of handling laboratory animals. The R94Q amino acid substitution was introduced by site-directed mutagenesis (QuickChange, Site-Directed Mutagenesis Kit, Stratagene) using the human *MFN2* cDNA as template (hMFN2). We sub-cloned the human *MFN2* R94Q cDNA into the neuron specific enolase promoter-Bcl2 plasmid (Martinou *et al.*, 1994) using the EcoR1 restriction site to obtain the neuron specific enolase promoter-MFN2R94Q construct. The neuron specific enolase promoter-hMFN2R94Q plasmid was linearized with Kpn1 and Xba1, purified and microinjected into the male pronucleus of B6D2F1 mouse fertilized oocytes. Genotyping of founder mice was done using MFN2 primers described previously (Cartoni *et al.*, 2005). The same procedure was followed to generate the hMFN2Wt mouse line.

Transgene expression analysis

Detection of transgene expression was done using reverse transcriptase polymerase chain reaction (PCR). RNA from tissues was extracted using TRI Reagent (Sigma) according to the manufacturer's instructions. One microgram of RNA was treated with RQ1 DNase (Promega) for 1 h and transformed into cDNA using M-MLV reverse transcriptase enzyme (Sigma) and random hexamer primers (Microsynth, CH). PCR was run on 200–500 ng of cDNA using human specific *MFN2* primers: forward, 5′-TGATGGGCTAC AATGACCAG-3′; reverse, 5′-AGCTTCTCGCTGGCATGC-3′. Relative quantification of human *MFN2* was performed by real time PCR using the ABI Prism 7500 real-time PCR system and SYBR Green (Applied Biosystems). All primers were designed to prevent amplification of genomic DNA. Cycling conditions were 95°C for 10 min, followed by 40 cycles of 95°C for 15 s and 60°C for 1 min. Quantification was performed using a standard curve established from a serial dilution of a mix of the samples. Results were normalized using the reference genes *Gapdh* (forward: 5′-ATCACCATCTTCCAGGAGCG-3′; reverse: 5′-GGCCTCACCCCATTTGATGT-3′). The histogram represents the results of technical triplicates. For each genotype, cDNAs of at least two individuals were pooled. To determine the expression of the transgene relative to the mouse endogenous *MFN2* expression, we performed PCR on cDNA, prepared as described earlier, using primers sharing complete sequence identity between mouse and human *Mfn2*. Forward, 5′-GAGCAGCTGGGGGCCTACATCCA-3′; reverse, 5′-CATT GATCACGGTGCTCTTCCCATTGCTCG-3′. The resulting 214 base pair PCR product was digested with XmnI enzyme specifically cutting the human PCR product into two fragments of 122 and 92 base pairs. Band intensity was measured using ImageJ software.

Behavioural tests

All animals were tested during the light phase of the light-dark cycle. All the experiments started at 2 p.m., after a 2 h habituation period

during which mice were placed in the testing room. When possible, transgenic mice were compared with their littermates. Isolated mice or pregnant females were excluded. Experiments were run blind. For the constant speed rotarod test (ROTA-ROD for mice 7650, Ugo Basile, Varese, Italy), mice were placed on the rotating rod spinning at a constant speed of 16 rpm. This speed was determined as the average latency reached by transgenic animals during preliminary accelerating rotarod tests. The latency to fall was measured individually. Each mouse performed three times and mice that reached 300 s were stopped.

The number of mice used for the mutant transgenic lines by age (1.5, 3 and 5 months) was: MitoCharc1, $n = 10$, 12 and 11; non-transgenic, $n = 9$, 8 and 8; MitoCharc2, $n = 7$, 7 and 7; non-transgenic, $n = 8$, 8 and 8. MitoCharc0 (5, 7 and 10 months): non-transgenic, $n = 6$, 6 and 6; MitoCharc0, $n = 8$, 8 and 8.

For the hind print test, non-toxic black paint was applied on the inside of the hind paws of the mice. Mice were placed on a paper sheet at the beginning of a narrow corridor (10 cm × 50 cm) and allowed to complete at least five complete steps.

Electron microscopy

Mice were perfused with 2% paraformaldehyde and 2% glutaraldehyde in 0.1 M cacodylate buffer (pH 7.3) for 5 min. The distal part of the sciatic nerve was dissected and post fixed by immersion in the fixative solution (2% paraformaldehyde, 2% glutaraldehyde, 0.1 M cacodylate buffer at pH 7.3) for 2 h at 4°C, and washed in 0.1 M cacodylate buffer, and osmicated for 4 h in 1% OsO_4 (Fluka). Nerves were rinsed in 0.1 M cacodylate buffer, dehydrated and embedded in epoxy 812-Araldite (Polysciences). Ultra-thin sections were subsequently cut, collected on cellodin-coated single slot grids and stained with uranyl acetate and lead citrate. Photographs were obtained using a Technai G2 electron microscope.

Morphometric analysis

Semi-thin (0.5 μm) nerve cross-sections were stained with 1% toluidine blue and digitalized using the AxioVision release 4.5 software (Zeiss). For each myelinated axon present, both an axonal area (defined by the inner limit of the myelin sheath) and a total fibre area (defined by the outer limit of the myelin sheath) were automatically measured using homemade image analysis software (Arnaud *et al.*, 2009). The g-ratio was calculated by dividing the axon area by total fibre area. The number of mice used were as follows: (i) 1.5 months: non-transgenic, $n = 4$, 6950 axons; MitoCharc1, $n = 4$, 7148 axons; (ii) 12 months: non-transgenic, $n = 5$, 2716 axons; MitoCharc1, $n = 5$, 3250 axons; (iii) 12 months: non-transgenic, $n = 4$, 3784 axons; MitoCharc2, $n = 3$ 3669 axons. Axonal density was measured from semi-thin nerve cross-sections used to determine axonal size of 12-month-old animals. Axonal area was set using ImageJ software and the number of axons was counted manually. The number of mice used was as follows: MitoCharc1, $n = 3$; non-transgenic, $n = 3$; MitoCharc2, $n = 3$; non-transgenic, $n = 4$.

Mitochondrial analysis

Axonal content of mitochondria was determined blind using electron microscopy pictures of axons. The number of structures identified as mitochondria as well as their integrity was determined for each sample. Individual axon size was measured using Freehand line tool of ImageJ software on the same electron microscopy pictures used for mitochondrial content evaluation allowing direct correlation of axonal diameter and mitochondrial content for each axon study.

The number of axons randomly considered (100 for each mouse) was sufficient to have the same proportion of small and big axons between transgenic and non-transgenic control. The number of mice used was as follows: (i) 1.5 months: MitoCharc1, $n = 4$; non-transgenic, $n = 4$; (ii) 12 months: MitoCharc1, $n = 3$; non-transgenic, $n = 4$; (iii) 12 months: MitoCharc2, $n = 3$; non-transgenic, $n = 4$.

Cerebellum histology

Mice were perfused as described in electron microscopy methods. Whole brain was dissected, embedded in Optimal Cutting Temperature compound (Tissue-Tek, Sakura) and immediately frozen in cold isopentane. Sagittal cryosections (10 μm) were stained with haematoxylin and eosin using standard procedures. For immunostaining, specimens were hybridized with anti-calbindin antibody (rabbit anti-Calbindin D-28k, CB-38a, Swant) following the procedure of the manufacturer. Briefly, anti-calbindin antibody (dilution 1:1000) was incubated 48 h, followed by 1 h incubation of bio-tinylated anti-rabbit IgG (H & L) (Vector, dilution 1:200) and 1 h Streptavidin, Alexa Fluor 594 conjugate antibody (Molecular Probe, dilution 1:200).

Compound action potential recording

Mice were anaesthetized with Isofluran (Baxter) and beheaded. Sciatic nerves were dissected and placed in artificial cerebrospinal fluid composed of (in mM): NaCl, 126; KCl, 3; NaH_2PO_4, 1.25; $CaCl_2$, 2; $MgCl_2$, 2; $NaHCO_3$, 26; glucose, 10; pH 7.4 (all salts from VWR), and continuously bubbled with carboxygen, a 95/5% mixture of O_2/CO_2. Nerves were allowed to equilibrate for 60 min before electrophysiological measurement.

For recordings, nerves were transferred to a homemade chamber perfused with artificial cerebrospinal fluid. Electrical stimuli were applied using a suction electrode at the proximal end of the nerve, and compound action potentials were recorded at the distal end with a pipette filled with artificial cerebrospinal fluid using a Multiclamp 700B amplifier (Molecular Devices). Signals were filtered and digitized with a Digidata 1440A (Molecular Devices). We used pClamp 10 for protocol generation, data acquisition and analysis. Nerve isolation and recordings were done at room temperature (20–22°C). For each component, we normalized the area by the amplitude to minimize the variability between experiments intrinsic to this technique (Stys *et al.*, 1991) and to differentiate the shape of the components. Number of mice used from 12 to 14 months: non-transgenic, $n = 10$, 15 nerves; MitoCharc1, $n = 6$, 10 nerves. All data are presented as mean ± SEM.

Statistics

For statistical analyses, we used a standard software package (R statistical software version 2.9.2). The effect of the rotarod task on the genotype was evaluated by means of repeated measurement analysis of variance (ANOVA). Mitochondria number data and axon size data were evaluated by Poisson and logistic regression, respectively. Compound action potentials were compared using unpaired Student's *t*-test.

Results

Generation of transgenic mice over-expressing human MFN2[R94Q] cDNA specifically in neurons

Whereas multiple forms of the demyelinating CMT disease (CMT1 and CMT4) have been investigated in detail through generations of several appropriate animal models (Scherer and Wrabetz, 2008), fewer studies have been devoted to the axonal form (CMT2). To generate a CMT2A mouse model, the human MFN2[R94Q] cDNA (hMFN2[R94Q]) or wild-type cDNA (hMFN2[Wt]) was cloned downstream to the neuron specific enolase promoter to ensure a pan-neuronal expression of the transgenic cDNA (Fig. 1A). This promoter was previously found to be selectively active in neurons of the peripheral and central nervous system, including motoneurons and dorsal root sensory ganglia, starting at E13 (Forss-Petter et al., 1990; Martinou et al., 1994). Using classical transgenic techniques, we obtained two lines that carried the neuron specific enolase-hMFN2[R94Q] transgene (hMFN2R94QL51, hMFN2R94QL87) and one carrying the neuron specific enolase-hMFN2[Wt] transgene (hMFN2WtL916). These three lines bred and produced offspring at the expected frequencies. Mutant and wild-type MFN2 did not bear any protein tag to avoid alteration of their function. To assess transgene expression in the different lines we rather took advantage of the difference between human and mouse Mfn2 nucleotide sequences. Using human MFN2 specific primers, reverse transcription PCR (RT-PCR) analysis showed that the three transgenic lines expressed the transgene selectively in neuronal tissues, including lumbar spinal cord and dorsal root sensory ganglia (Fig. 1B). We named the mutant line hMFN2R94QL51 MitoCharc1. Because the mutant line hMFN2R94QL87, heterozygous for the transgene, did not show any pathological phenotype (data not shown), transgenic mice from this line were bred to obtain homozygous animals. We named this homozygous MFN2R94QL87 line MitoCharc2. The transgenic line hMFN2WtL916 was called MitoCharc0. To evaluate the expression level of the hMFN2R94Q transgene in comparison to endogenous Mfn2 in MitoCharc1 and 2 mice, we used a semi-quantitative RT-PCR approach. Primers sharing identical sequence between mouse and human MFN2 transcripts were used to obtain reverse transcriptase polymerase chain reaction products from dorsal root ganglion and spinal cord of transgenic mice. A digestion with XmnI generated two bands of 122 and 92 bp from amplicons derived from human MFN2, while amplicons derived from mouse Mfn2 remained intact (band of 214 bp, Fig. 1C and D). Quantification of these results revealed a moderate level of transgene overexpression varying from 1.1 to 4.6 times as compared with endogenous Mfn2 expression (Supplementary Fig. 1A). To compare the level of expression of the hMFN2R94Q and the wild-type transgene in the corresponding transgenic lines, we also performed quantitative real time RT-PCR using human specific MFN2 primers. Importantly, the MitoCharc0 line revealed a level of expression higher than the level in the two mutant lines making it a good control line to
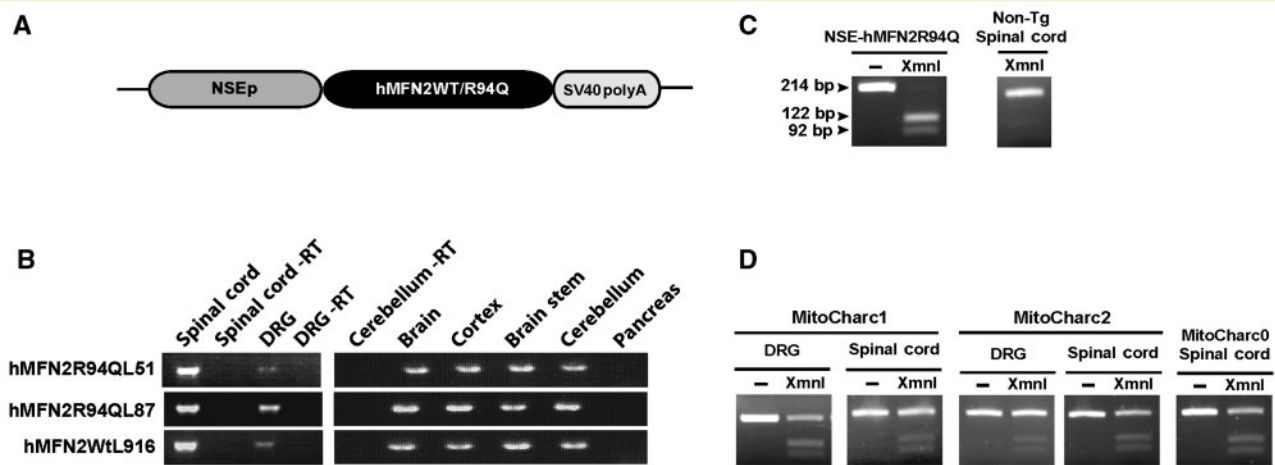

Figure 1 Generation of MitoCharc mice. (**A**) Schematic representation of the construct used to generate MitoCharc mice. Human cDNAs containing either wild-type or the mutated form of MFN2 (R94Q) were cloned downstream to the neuron specific enolase promoter (NSEp) to ensure a neuron specific expression of the transgene. (**B**) Transgene expression was measured by reverse transcriptase (RT) PCR using human specific MFN2 primers. Reverse transcription was performed on RNA extracts from several tissues isolated from hMfn2R94QL51, hMfn2R94QL87 and hMfn2Wt mice (-RT samples are controls where no reverse transcriptase was added). All lines expressed the transgene in neuronal tissues. (**C** and **D**) Transgene expression relative to endogenous Mfn2. The human MFN2 reverse transcriptase PCR product (214 bp) is specifically cut by XmnI digestion leading to the detection of two lower bands of 122 and 92 bp. (**C**) The first panel shows the complete digestion of the human MFN2 PCR product obtained from the plasmid neuron specific enolase-hMFN2R94Q, and the absence of digestion fragments in reverse transcriptase PCR products from spinal cord of the non-transgenic (Non-Tg) mouse (second panel). (**D**) XmnI digestion of reverse transcriptase PCR product from the indicated tissue of MitoCharc1, 2 and 0 mice. All the lines showed a moderate level of expression of the transgene.

evaluate the effect of wild-type MFN2 overexpression in neurons (Supplementary Fig. 1B).

MitoCharc mice as a model of CMT2A

The first symptoms of patients with MFN2-related CMT2A are locomotor impairments such as difficulty in walking and frequent falls (Verhoeven *et al.*, 2006). We therefore tested the motor capacities of MitoCharc mice using a rotarod test (Fig. 2A). Whereas we could not detect any difference between mutant and control animals at 1.5 and 3 months of age, at 5 months of age both MitoCharc1 and 2 mice performed less well compared to control non-transgenic littermates and age-matched controls ($P = 0.0082$ and 0.0084, respectively). The progressive aspect of this phenotype was confirmed by a significant difference when comparing the performance at 1.5 versus 5 months in the two mutant lines (MitoCharc1 $P<0.001$ and MitoCharc2 $P=0.001$). Interestingly, while MitoCharc1 mice displayed a quite homogeneous phenotype at 5 months of age there was a substantial phenotypic variation among the MitoCharc2 mice (Fig. 2A).

These data suggest a non-complete phenotypic penetrance in MitoCharc2 mice. By 5 months of age, some animals from the MitoCharc2 line developed a very striking motor deficit. As depicted in Fig. 2B (left panel), they stood very low on their legs and displayed a dragging tail. This position induced a gait defect as shown in Fig. 2B (right panel) in a representative hind print test. Affected MitoCharc2 mice walked with shorter steps and with everted paws. Thus, although MitoCharc1 and 2 lines showed similar rotarod impairments, their neurological phenotype was not identical, probably because of the different transgene expression levels (Supplementary Fig. 1). Importantly, the MitoCharc0 transgenic mice did not show any phenotype in the rotarod test, strongly suggesting that the observed phenotype in MitoCharc1 and 2 is a consequence of the expression of the R94Q mutated form of MFN2 in these animals (Supplementary Fig. 2). Because cerebellum degeneration has been reported in *Mfn2* null mice (Chen et al., 2007), we investigated its integrity in MitoCharc1 mice. Consistent with the lack of ataxic phenotype in both MitoCharc1 and 2 mice, we did not observe any morphological defects of the cerebellum in transgenic animals when compared to
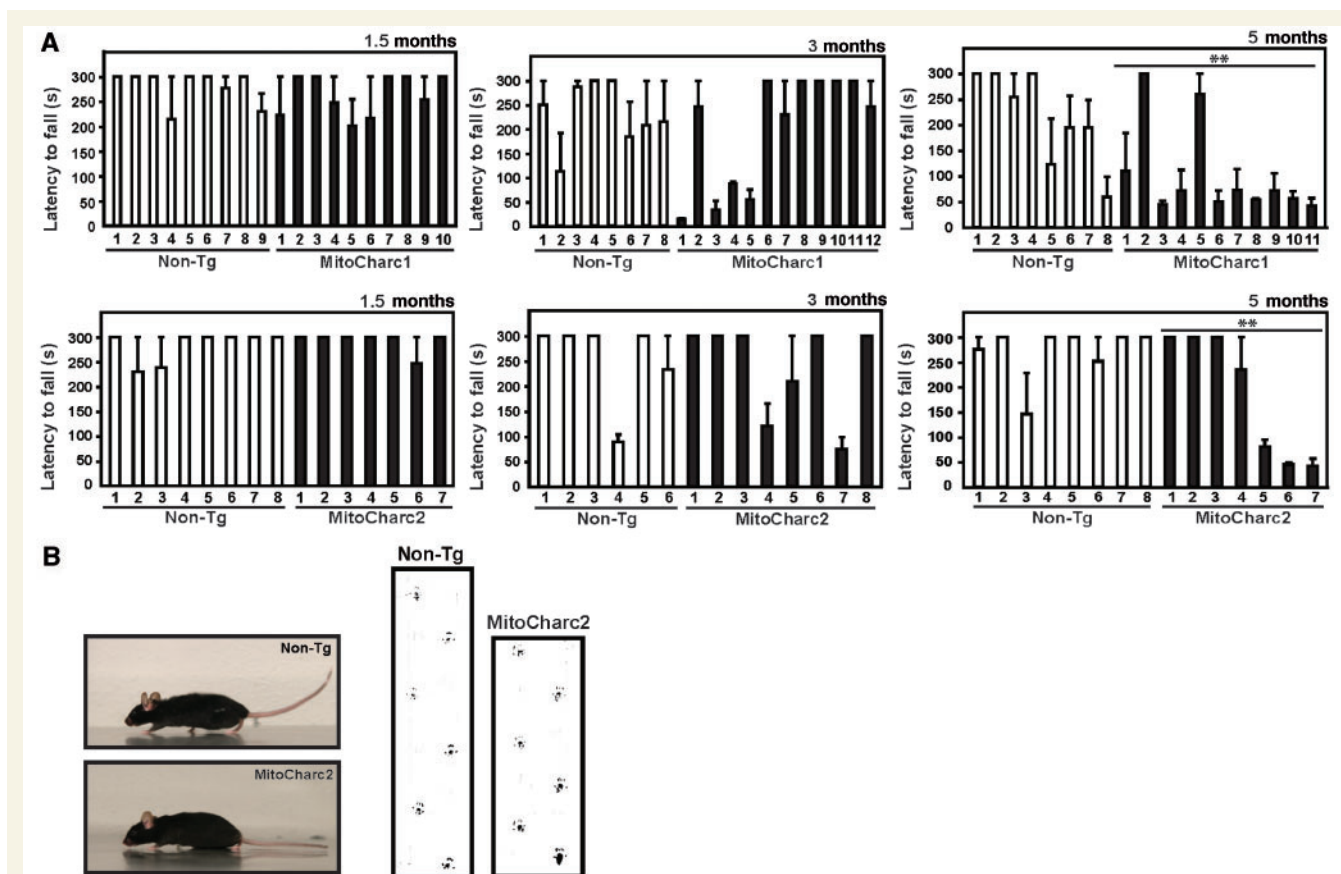

Figure 2 CMT2A-like phenotype in MitoCharc1 and 2 mice. (**A**) Constant speed rotarod test results of adult MitoCharc1, 2 and their wild-type littermate and non-transgenic (Non-Tg) controls, respectively. From 5 months of age, MitoCharc1 and 2 mice show marked locomotor defects. The mean of three trials is represented for each individual mouse. (**B**) Adult diseased MitoCharc2 mice displayed a phenotype characterized by a low body position and a dragging tail (left panels). The right panels show a representative hind print test depicting a gait defect at the same age. Diseased MitoCharc2 mice walked with shorter steps and everted paws. Statistically significant differences are indicated by **$P<0.01$. Error bars = SEM.

non-transgenic controls. Molecular, Purkinje and granular layers displayed a normal appearance (Supplementary Fig. 3).

Increased number of mitochondria in the peripheral nervous system axons of MitoCharc mutant mice

While the number of mitochondria is increased in distal axons of patients with CMT2A (Verhoeven et al., 2006; Vallat et al., 2008; Funalot et al., 2009), this abnormality has not been observed in the previously reported in vivo or in vitro models of CMT2A (Baloh et al., 2007; Detmer et al., 2008). Since MFN2 plays a role in mitochondrial fusion (Chen et al., 2003), we evaluated the morphology and distribution of mitochondria in the soma of motoneurons and axons of the sciatic nerve by electron microscopy. We could not detect any morphological abnormality or aggregation of mitochondria in motoneuron cell bodies of 1-year-old MitoCharc1 mice (Supplementary Fig. 4). In contrast, we observed that in the medium and small myelinated axons (diameter $<3.5\,\mu m$) of both MitoCharc1 and 2 mice, the number of mitochondria per axon, as compared to controls, was significantly increased (34%, $P=0.007$ and 28%, $P=0.011$, respectively; Fig. 3A and B). The number of mitochondria per axon did not change in larger myelinated axons (diameter $>3.5\,\mu m$) in either mutant line. Mitochondrial ultrastructure, as analysed by electron microscopy, was not different in large or small axons in the sciatic nerve of MitoCharc1 and 2 mice when compared with their respective controls (data not shown).

In order to assess whether the increased number of mitochondria correlated with locomotor impairments, we also analysed sciatic nerves from asymptomatic, 1.5-month-old MitoCharc1 mice. Interestingly, the number of mitochondria in axons of these mice was not different from the number of mitochondria in axons of control non-transgenic littermates (Fig. 3A and B, left panels) suggesting a link between accumulation of mitochondria and the motor phenotype displayed by older mutant animals.

Axonal calibre defect in the distal part of sciatic nerves from MitoCharc mice

To investigate further the possible relation between increased mitochondrial number in the axons and the appearance of locomotor defects in older mutant animals, we analysed in detail the axonal morphology in sciatic nerves from 12-month-old transgenic and control mice. No major axonal or Schwann cell degeneration pattern was observed in either genotype at the light microscopic level (Fig. 4A). Consistent with the axonal neuropathy phenotype displayed by CMT2A patients, the g-ratio measuring the size ratio between area of axoplasm and myelin sheath was similar between MitoCharc1 and 2 mice, and respective controls demonstrating preservation of normal myelin thickness in mutant animals (Fig. 4B). The axonal density was also normal in transgenic mice indicating no gross axonal degeneration (Supplementary Fig. 5). Since especially late onset CMT2A patients do not necessarily display gross axonal degeneration (Chung et al., 2006), we investigated the sciatic nerve axonal morphology in more detail. We

performed a morphometric analysis of axons in the distal part of the sciatic nerves from MitoCharc1 and 2 mice (Fig. 4C). In 1.5-month-old asymptomatic MitoCharc1 mice, we did not detect any change in axonal distribution as compared to their control non-transgenic littermates. However, we observed a 40% ($P<0.001$) and 55% ($P<0.001$) increase in the proportion of small and medium sized axons and a consequent decrease in the proportion of larger axons in 12-month-old MitoCharc1 and 2 animals, respectively. Importantly, the switch of the axonal distribution curve of 12-month-old MitoCharc mice occurred approximately at the axonal diameter of $3.5\,\mu m$ that corresponds to the cut-off size under which we detected axonal mitochondrial accumulation (Fig. 3). We then tested whether the increase in the proportion of small–medium axons in the sciatic nerves of MitoCharc1 could be confirmed functionally by means of electrophysiological measurements. We measured sciatic nerve A fibre compound action potentials (Stys et al., 1991) in 12- to 16-month-old non-transgenic control and MitoCharc1 animals. As previously described, we were able to generate a fast and large response corresponding essentially to large diameter Aα/β fibres as well as a delayed, small peak corresponding mainly to Aδ fibres (Supplementary Fig. 6) (Waxman et al., 1995). We observed a slight non-significant decrease in Aα/β component area (Supplementary Table 1A) in the sciatic nerves of MitoCharc1 mice related to a similar change in their amplitude. The ratio area/amplitude, the decay slope, and the length of the Aα/β response in MitoCharc1 were normal (Fig. 4D, left panel and Supplementary Table 1). Interestingly, the Aδ fibres component was altered in the sciatic nerves of MitoCharc1. Compound action potential amplitude was stable but its average area augmented. The area/amplitude ratio increased significantly suggesting a change in the shape of the Aδ component (Fig. 4D, right panel). Accordingly, we observed a significant slow down of the decay (Supplementary Table 1B) that can be correlated to the change in area. It is likely that this higher area and the slow down of the Aδ component are due to an increase in the number of Aδ-like fibres.

Discussion

In this report, we describe the generation and characterization of a mouse model of the CMT2A peripheral neuropathy induced by a R94Q mutation in MFN2. We propose that the motor defects observed in MitoCharc mutant mice are related to the altered axonal mitochondrial density that may underlie changes in axonal size distribution.

In previous attempts to build murine models of CMT2A, over-expression of mutant MFN2 led to an accumulation of mitochondria in the soma of motoneurons and, consequently, to a depletion of these organelles in axons (Detmer et al., 2008). This altered cellular topology of mitochondria was probably not linked to the nature of the MFN2 mutations that were used in these studies but rather to the expression of a high level of the MFN2 protein. Indeed, an alteration in the cellular topology of mitochondria, with aggregation of mitochondria around the nucleus, has also been observed when wild-type or mutant forms of MFN2 or
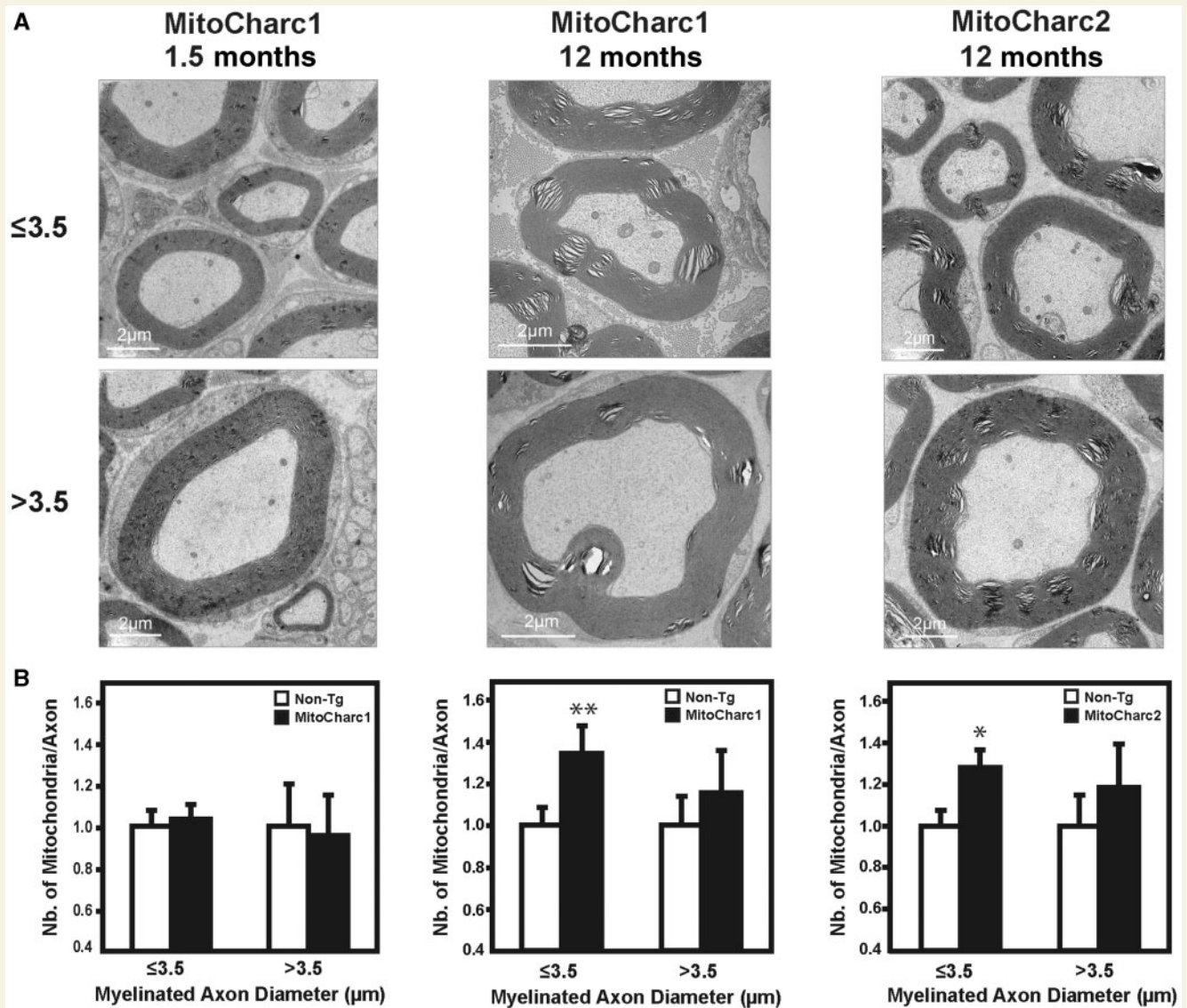
Figure 3 Increased number of mitochondria in the distal part of the sciatic nerve from MitoCharc1 and 2 mice. (**A**) Mitochondria axonal content was quantified by electron microscopy analysis of distal cross sections of sciatic nerve. At 12 months of age, MitoCharc1 and 2 mice showed an increase in the number of mitochondria in axons with diameter smaller than 3.5 μm. Asymptomatic MitoCharc1 mice (1.5 months old) did not show any change in the mitochondrial pattern. (**B**) Quantification of the relative number of mitochondria per axon in MitoCharc and non-transgenic (Non-Tg) mice. In small–medium axons of 12-month-old MitoCharc1 and 2 mice, the number of mitochondria was significantly increased by 34 and 28%, respectively. Error bars = SEM, statistically significant differences are indicated by *$P<0.05$ and **$P<0.01$.

MFN1 were highly expressed in cultured cells (Eura et al., 2003). In our studies, we did not observe an axonal depletion of mitochondria, probably because the level of transgene expression conferred by the neuron specific enolase promoter is moderate (1.1- to 4.6-fold overexpression) and relatively close to the expected expression level of mutant MFN2 in neurons from human patients. Rather, the number of mitochondria in axons of the sciatic nerve was increased by ∼30% in mice expressing mutant MFN2. This observation is consistent with the ultrastructural analysis of the sural nerve in patients with CMT2A that also revealed an accumulation of axonal mitochondria (Verhoeven et al., 2006; Vallat

et al., 2008; Funalot et al., 2009). To our knowledge, this is the first time that this key feature of CMT2A, due to an MFN2 mutation, is observed in a mouse model. The increase in mitochondrial density observed in the distal axons of MitoCharc mutant mice, as well as in patients with CMT2A, can have several origins, including a defect in the retrograde transport of mitochondria, an increase in the total number of mitochondria or a raise in the number of the fission events leading to an increased number of organelles without affecting the total mitochondrial mass. Because MFN2 is known to play a role in the fusion of the outer mitochondrial membrane and mitofusins are required for mitochondrial
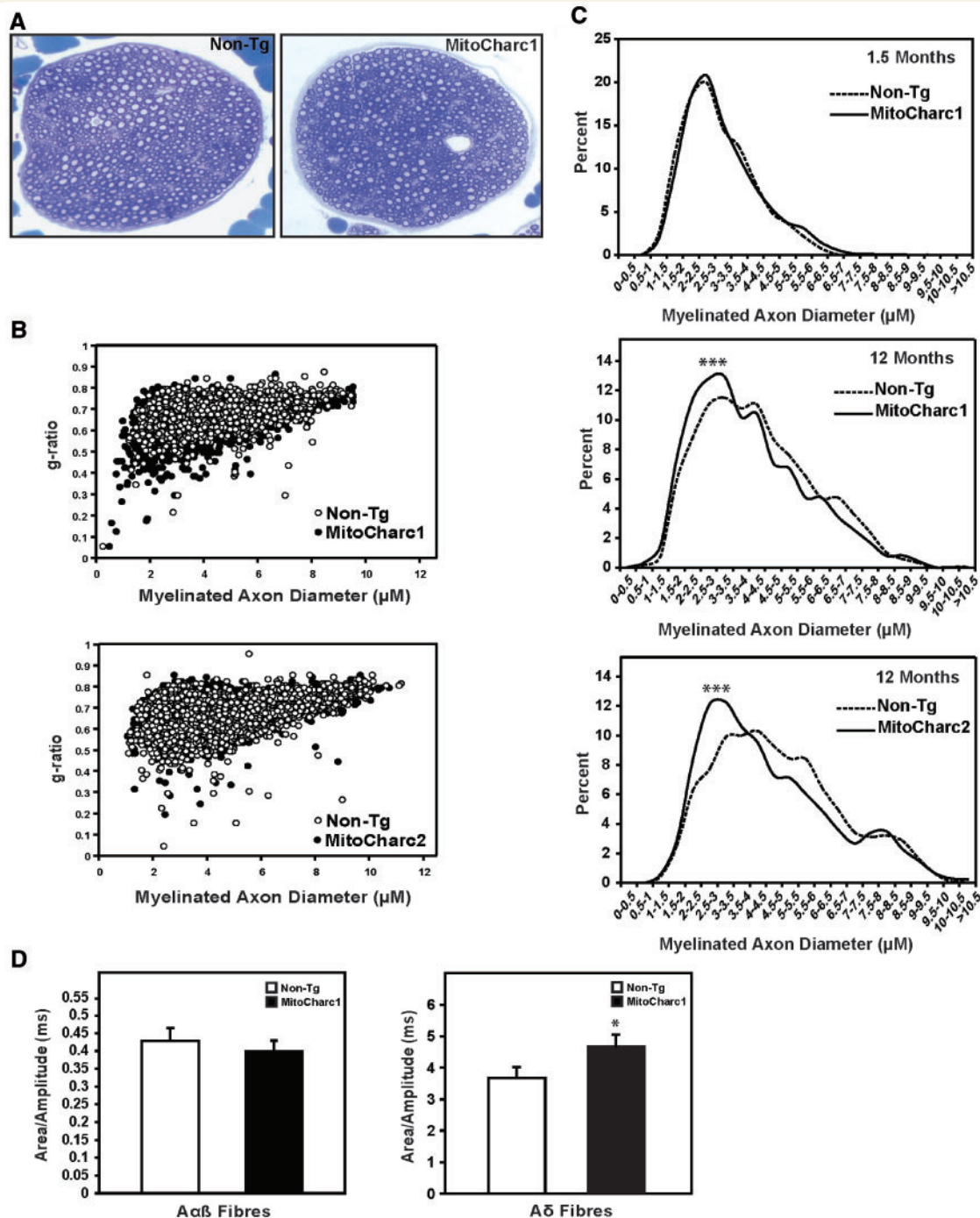
Figure 4 Axonopathy in the peripheral nervous system of MitoCharc1 and 2 mice. (**A**) Semi-thin cross sections of MitoCharc1 and non-transgenic (Non-Tg) sciatic nerves stained with toluidine blue. (**B**) g-ratio analysis of 12-month-old MitoCharc mice. As revealed by identical g-ratios between transgenic and non-transgenic animals no myelinization defect was observed in MitoCharc1 and 2 mice. Number of animals (*n*) and number of axons measured are the same as in **C**. (**C**) Morphometric analysis of axons from MitoCharc1 and 2 mice as compared to non-transgenic controls. At 1.5 months of age, no difference was observed between the axonal repartition of MitoCharc1 mice as compared to non-transgenic controls (upper panel). At 12 months of age, the axonal distribution pattern revealed an over representation of small–medium axons ($<3.5\,\mu m$) in both MitoCharc1 (middle panel) and MitoCharc2 (lower panel) mice. The proportion of small–medium axons was increased by 40 and 55% in MitoCharc1 and MitoCharc2 mice, respectively. (**D**) Electrophysiological analysis of MitoCharc1 and non-transgenic control sciatic nerves. The component area/amplitude ratio generated by the large A$\alpha\beta$ (left panel) and small–medium fibres Aδ (right panel) showed a significant increase in Aδ component ratio of MitoCharc1 mice. Statistically significant differences are indicated by $*P<0.05$ and $***P<0.001$.

fusion, we favour the hypothesis of a mitochondrial fusion defect, even though an impairment of mitochondrial motility cannot be excluded. In support of this hypothesis, MFN2[R94Q] has been shown to be non-functional for fusion in a context where MFN1 cannot complement the fusion activity (Detmer and Chan, 2007a). Moreover, neurons express less MFN1 than MFN2 (for example Purkinje cells or dorsal root ganglion neurons), which makes mitochondria in these cells more vulnerable to MFN2 mutations (Detmer and Chan, 2007a; R. Cartoni, unpublished observation).

Another aspect of the phenotype that distinguishes the MFN2[R94Q] transgenic mice from previously published models is the relatively late onset of their neuropathy. Both at the functional level (rotarod and gait defects) and at the histological level (axonal accumulation of mitochondria and shift in axonal size distribution), only MitoCharc mice ≥ 5 months of age became symptomatic. These data, together with the absence of prominent muscle atrophy, therefore suggest that MitoCharc1 and 2 transgenic mice represent a model of a late onset CMT2A (Chung *et al.*, 2006). Finally, in the MitoCharc1 and 2 mice the neuron specific enolase promoter is active from embryogenesis until adulthood whereas in the published model by Detmer *et al.* (2008), the HB9 motoneuron-specific promoter is only active until the post-natal period (P6), which could explain an acute effect on motoneuron development. The sciatic nerves from MitoCharc1 and 2 mice display an over representation of small calibre axons in aged animals. Because compound action potential area is proportional to the number of activated fibres and to the square of their diameters (Keynes and Aidley, 2001), we used compound action potential recordings on sciatic nerve explants to test whether the increased proportion of small–medium calibre axons had an impact on the electrophysiological recordings of the sciatic nerve. We observed a significant increase of the area/amplitude ratio for Aδ fibres due to a significant slow down of the decay (Fig. 4D and Supplementary Table 1B). As Aδ component corresponds to the trace generated by small–medium diameter fibres, these data corroborate with the increase in the proportion of small and medium sized axons observed in the sciatic nerves of MitoCharc1 mice. We did not observe a significant decrease in A$\alpha\beta$ component area and amplitude in the sciatic nerve of MitoCharc1. This is in line with our data from morphometric analysis, since the largest (Aα) fibres are the major contributors of the A$\alpha\beta$ component and we did not observe any changes in the Aα axons of the MitoCharc1. While we did not observe axonal distribution change at 1.5 months of age (developmental stage at which the peripheral system already acquired its functional architecture), the increase in small axonal fibres still may be a consequence of impaired axonal radial growth since the process of axonal maturation continues even in older animals (see difference in axonal distribution at 1.5 and 12 months of age in Fig. 4C). Alternatively, axonal atrophy of larger axons may also lead to the observed over representation of smaller axons as previously suggested in other CMT models (Seburn *et al.*, 2006). Mitochondrial fission due to disruption of the *Mfn2* gene in the mouse, and consequent dysfunction of these organelles, has previously been reported to be responsible for neurite atrophy of Purkinje cells (Chen *et al.*, 2007). This suggests that mitochondrial fusion impairment could be responsible for the change in the size of axons in the sciatic nerve of MitoCharc mice. In support of this hypothesis, the protein affected in autosomal dominant optic atrophy neuropathy, in which atrophy of the optic nerve is the main symptom, is optic atrophy 1 (OPA1), a protein responsible for the fusion of the inner mitochondrial membrane (Alexander *et al.*, 2000; Delettre *et al.*, 2000; Amati-Bonneau *et al.*, 2009). Fibroblasts from patients carrying OPA1 mutation display partial or complete fragmentation of the mitochondrial network suggesting that mitochondrial network alteration could be the cause of optic nerve atrophy (Amati-Bonneau *et al.*, 2009). Importantly, similar to our results in MitoCharc mutant mice, the late onset symptomatic CMT2A patients carrying MFN2 mutations do not present any sign of obvious axonal loss as evaluated in sural nerve biopsies (Chung *et al.*, 2006). Whether axonal atrophy, as observed in MitoCharc animals, is present in nerves of late onset CMT2A patients and if this contributes to their symptomatology remains to be assessed.

In conclusion, we have generated transgenic mice overexpressing in neurons a mutant or wild-type form of MFN2. Because only mice expressing mutant MFN2 display clinical symptoms reminiscent of CMT2A, we think that the cause of these symptoms can unambiguously be assigned to the MFN2[R94Q] mutation. These mice represent an interesting tool to further explore the physiopathology of CMT2A disease and should make possible the evaluation of future therapeutic approaches.

Acknowledgements

Funding

Supplementary material

Supplementary material is available at *Brain* online.

References

Alexander C, Votruba M, Pesch UE, Thiselton DL, Mayer S, Moore A, et al. OPA1, encoding a dynamin-related GTPase, is mutated in autosomal dominant optic atrophy linked to chromosome 3q28. Nat Genet 2000; 26: 211–5.

Amati-Bonneau P, Milea D, Bonneau D, Chevrollier A, Ferre M, Guillet V, et al. OPA1-associated disorders: phenotypes and pathophysiology. Int J Biochem Cell Biol 2009; 41: 1855–65.

Arnaud E, Zenker J, DePreux Charles A, Stendel C, Roos A, Medard J, et al. SH3TC2/KIAA1985 protein is required for proper myelination and the integrity of the node of Ranvier in the peripheral nervous system. Proc Natl Acad Sci USA 2009; 106: 17528–33.

Baloh RH, Schmidt RE, Pestronk A, Milbrandt J. Altered axonal mitochondrial transport in the pathogenesis of Charcot-Marie-Tooth disease from mitofusin 2 mutations. J Neurosci 2007; 27: 422–30.

Cartoni R, Martinou JC. Role of mitofusin 2 mutations in the physiopathology of Charcot-Marie-Tooth disease type 2A. Exp Neurol 2009; 218: 268–73.

Cartoni R, Leger B, Hock MB, Praz M, Crettenand A, Pich S, et al. Mitofusins 1/2 and ERRalpha expression are increased in human skeletal muscle after physical exercise. J Physiol 2005; 567: 349–58.

Chan DC. Mitochondrial fusion and fission in mammals. Annu Rev Cell Dev Biol 2006; 22: 79–99.

Chen H, Detmer SA, Ewald AJ, Griffin EE, Fraser SE, Chan DC. Mitofusins Mfn1 and Mfn2 coordinately regulate mitochondrial fusion and are essential for embryonic development. J Cell Biol 2003; 160: 189–200.

Chen H, McCaffery JM, Chan DC. Mitochondrial fusion protects against neurodegeneration in the cerebellum. Cell 2007; 130: 548–62.

Chung KW, Kim SB, Park KD, Choi KG, Lee JH, Eun HW, et al. Early onset severe and late-onset mild Charcot-Marie-Tooth disease with mitofusin 2 (MFN2) mutations. Brain 2006; 129: 2103–18.

Delettre C, Lenaers G, Griffoin JM, Gigarel N, Lorenzo C, Belenguer P, et al. Nuclear gene OPA1, encoding a mitochondrial dynamin-related protein, is mutated in dominant optic atrophy. Nat Genet 2000; 26: 207–10.

Detmer SA, Chan DC. Complementation between mouse Mfn1 and Mfn2 protects mitochondrial fusion defects caused by CMT2A disease mutations. J Cell Biol 2007a; 176: 405–14.

Detmer SA, Chan DC. Functions and dysfunctions of mitochondrial dynamics. Nat Rev Mol Cell Biol 2007b; 8: 870–9.

Detmer SA, Vande Velde C, Cleveland DW, Chan DC. Hindlimb gait defects due to motor axon loss and reduced distal muscles in a transgenic mouse model of Charcot-Marie-Tooth type 2A. Hum Mol Genet 2008; 17: 367–75.

Eura Y, Ishihara N, Yokota S, Mihara K. Two mitofusin proteins, mammalian homologues of FZO, with distinct functions are both required for mitochondrial fusion. J Biochem (Tokyo) 2003; 134: 333–44.

Forss-Petter S, Danielson PE, Catsicas S, Battenberg E, Price J, Nerenberg M, et al. Transgenic mice expressing beta-galactosidase in mature neurons under neuron-specific enolase promoter control. Neuron 1990; 5: 187–97.

Funalot B, Magdelaine C, Sturtz F, Ouvrier R, Vallat JM. Ultrastructural lesions of axonal mitochondria in patients with childhood-onset Charcot-Marie-Tooth disease due to MFN2 mutations. Bull Acad Natl Med 2009; 193: 151–60; discussion 160–1.

Keynes RD, Aidley DJ. Nerve and Muscle. Cambridge: Cambridge University Press; 2001.

Kijima K, Numakura C, Izumino H, Umetsu K, Nezu A, Shiiki T, et al. Mitochondrial GTPase mitofusin 2 mutation in Charcot-Marie-Tooth neuropathy type 2A. Hum Genet 2005; 116: 23–7.

Martinou JC, Dubois-Dauphin M, Staple JK, Rodriguez I, Frankowski H, Missotten M, et al. Overexpression of BCL-2 in transgenic mice protects neurons from naturally occurring cell death and experimental ischemia. Neuron 1994; 13: 1017–30.

Scherer SS, Wrabetz L. Molecular mechanisms of inherited demyelinating neuropathies. Glia 2008; 56: 1578–89.

Schröder JM. Pathology of peripheral nerves: an atlas of structural and molecular pathological changes. Berlin: Springer; 2001.

Seburn KL, Nangle LA, Cox GA, Schimmel P, Burgess RW. An active dominant mutation of glycyl-tRNA synthetase causes neuropathy in a Charcot-Marie-Tooth 2D mouse model. Neuron 2006; 51: 715–26.

Skre H. Genetic and clinical aspects of Charcot-Marie-Tooth's disease. Clin Genet 1974; 6: 98–118.

Stys PK, Ransom BR, Waxman SG. Compound action potential of nerve recorded by suction electrode: a theoretical and experimental analysis. Brain Res 1991; 546: 18–32.

Vallat JM, Ouvrier RA, Pollard JD, Magdelaine C, Zhu D, Nicholson GA, et al. Histopathological findings in hereditary motor and sensory neuropathy of axonal type with onset in early childhood associated with mitofusin 2 mutations. J Neuropathol Exp Neurol 2008; 67: 1097–102.

Verhoeven K, Claeys KG, Zuchner S, Schroder JM, Weis J, Ceuterick C, et al. MFN2 mutation distribution and genotype/phenotype correlation in Charcot-Marie-Tooth type 2. Brain 2006; 129: 2093–102.

Waxman SG, Kocsis JD, Stys PK. The axon : structure, function and pathophysiology. New York: Oxford: Oxford University Press; 1995.

Zuchner S, Mersiyanova IV, Muglia M, Bissar-Tadmouri N, Rochelle J, Dadali EL, et al. Mutations in the mitochondrial GTPase mitofusin 2 cause Charcot-Marie-Tooth neuropathy type 2A. Nat Genet 2004; 36: 449–51.